

<sup>1</sup> e-mail: christoph.naegerl@uibk.ac.at

**Key words** Bose-Einstein condensation

arXiv:cond-mat/0408268v1 [cond-mat.other] 12 Aug 2004<sup>2</sup>

# Optimized production of a cesium Bose-Einstein condensate

Tobias Kraemer<sup>1</sup>, Jens Herbig<sup>1</sup>, Michael Mark<sup>1</sup>, Tino Weber<sup>1</sup>, Cheng Chin<sup>1</sup>, Hanns-Christoph Nägerl<sup>1\*</sup>, and Rudolf Grimm<sup>1,2</sup>

<sup>1</sup>Institut für Experimentalphysik, Universität Innsbruck, Technikerstraße 25, A-6020 Innsbruck, Austria

<sup>2</sup>Institut für Quantenoptik und Quanteninformation, Österreichische Akademie der Wissenschaften, A-6020 Innsbruck, Austria

Received: date / Revised version: date

**Abstract** We report on the optimized production of a Bose-Einstein condensate of cesium atoms using an optical trapping approach. Based on an improved trap loading and evaporation scheme we obtain more than  $10^5$  atoms in the condensed phase. To test the tunability of the interaction in the condensate we study the expansion of the condensate as a function of scattering length. We further excite strong oscillations of the trapped condensate by rapidly varying the interaction strength.

**PACS:** 03.75.Kk; 32.80.Pj

## 1 Introduction

Much of the present work in the field of quantum gases relies on optical trapping techniques and on the ability to tune atomic interactions. Optical approaches have been recently employed in several atomic Bose-Einstein condensation experiments [1, 2, 3, 4, 5] and in experiments on the production of ultracold molecular samples [6, 7, 8, 9, 10] and on molecular Bose-Einstein condensates [11, 12]. The major advantages in optical traps are the possibility to trap atoms in any sublevel of the electronic ground state and the ease to adjust the interaction strength using magnetically induced Feshbach resonances.

The cesium atom is very attractive for experiments with tunable atomic interactions. The lowest internal quantum state of Cs features a unique combination of wide and narrow Feshbach resonances which are easily accessible at low magnetic fields [13]. This results in a great flexibility for tuning the atomic scattering properties. In particular, magnetic tuning of the interaction strength has recently allowed the first realization of a Bose-Einstein condensate (BEC) with Cs atoms [4] and the realization of a two-dimensional condensate very close to a dielectric surface [5]. The tunability of the atomic interaction can be exploited in experiments where one might wish to adjust or to dynamically change the mean-field interaction of the condensate. Also, the Feshbach resonances can be used to produce molecules from an atomic BEC [14, 8,

9, 10] and to study the transition from an atomic BEC to a molecular BEC. In this context, a quantum phase transition with an essentially topological character has been predicted [15, 16]. For such and many other intriguing experiments it is desirable to have a large BEC of Cs atoms as a starting point.

In this paper we report on the optimized production of an essentially pure Cs BEC in the lowest internal quantum state with more than  $10^5$  atoms. Since this state cannot be trapped by purely magnetic means, the path to condensation relies on a sequence of optical traps. We discuss the loading and transfer from one trap to the next and give a detailed description of the evaporation path and of the resulting condensate. As a demonstration for tunability we measure the expansion energy as a function of scattering length in time-of-flight experiments. In particular, we show the ultra-slow expansion of the condensate after release from the trap for nearly vanishing scattering length. The release energy corresponds to  $\sim 50$  pK. Finally, we present first results when the scattering length is suddenly stepped and the condensate then starts to oscillate freely in the trap.

## 2 Cesium scattering properties and Feshbach resonances

Early experiments [17, 18] towards condensation of cesium focused on samples in magnetic traps polarized either in the upper hyperfine ground state  $F = 4$ , magnetic sublevel  $m_F = 4$ , or in the lower hyperfine state  $F = 3$ ,  $m_F = -3$ . Here,  $F$  denotes the total angular momentum and  $m_F$  the magnetic quantum number. The spin relaxation rates were measured to be several orders of magnitude higher than expected [19, 20, 21]. It was later understood that this is caused by the dipolar relaxation process induced by the second-order spin-orbit interaction [22]. The maximum phase-space density in a small sample of Cs atoms was a factor of about four away from condensation [23].

The problem of the strong inelastic two-body losses can be overcome by using the lowest internal state of cesium,

\* corresponding author

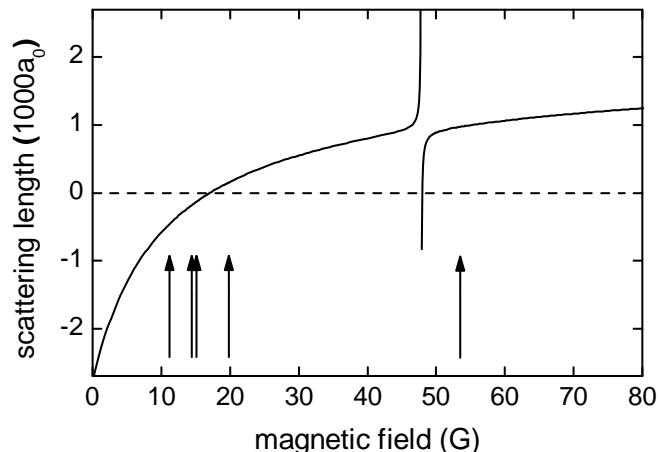


**Fig. 1** Scattering length as a function of magnetic field for the state  $F = 3, m_F = 3$ . There is a relatively broad Feshbach resonance at 48.0 G due to coupling to a d-wave molecular state. The arrows indicate several very narrow resonances at 11.0, 14.4, 15.0, 19.9 and 53.5 G, which result from coupling to g-wave molecular states. The data is taken from [13].

energy according to energy and momentum conservation. The atoms that form the molecule are usually lost, and the third atom is either lost or it deposits its share of the binding energy in the sample. Heating of the sample is the combination of “anti-evaporation” and recombination heating [28]. To a good approximation, the three-body recombination rate scales with the fourth power of the scattering length. Unfortunately, the prefactor in this scaling law is measured to be relatively large [28]. To minimize this heating, the recombination products should be removed quickly from the trap. It is thus important to assure that the sample is not operated too deep in the hydrodynamic regime and that the evaporation is efficient in *all* directions. Arbitrarily increasing the scattering length to speed up the forced evaporation is therefore not possible without sacrificing cooling efficiency. Within these limits, tuning the scattering length allows for an optimization of the evaporation for given trap parameters. For example, for the low initial densities in a large reservoir trap the evaporation may be sped up by increasing the scattering length. In a later trapping stage with a higher atomic density the scattering length should be reduced to optimize the ratio of good to bad collisions.

### 3 BEC production

#### 3.1 Overview of experimental strategy

For producing large condensates in optical dipole traps, it is necessary to independently optimize both trap loading and evaporative cooling. For initial loading of as many atoms as possible, an optical trap with large volume is needed which, in view of limited laser power, implies a shallow trapping potential. For subsequent forced evaporative cooling, however, high densities and fast elastic collisions require much tighter confinement. These two requirements in general demand dynamical changes of the trapping potential. A possible way to implement this is a spatial compression of the optical trap using e.g. a zoom-lens system [29]. Our approach is based on an alternative way where a sequence of optical trapping schemes is used to provide optimized loading together with optimized evaporative cooling.

We first use a shallow, large volume CO<sub>2</sub>-laser trap as a “reservoir” for collecting the atoms before forced evaporative cooling is implemented in a tighter trap. The reservoir trap can be efficiently loaded with atoms that are precooled by Raman-sideband cooling [30]. This approach allows collection of atoms at moderate densities with little loss from three-body collisions and with negligible heating from either photon scattering or trap vibrations. It serves as a good starting point for the final transfer into a tighter optical trap. The tighter trap is adiabatically increased and adds a “dimple” to the trapping potential of the reservoir. Collisional loading of this dimple already yields a significant enhancement of the local number and phase-space density [31]. After turn-

1  $F = 3, m_F = 3$  [24,25,26,27]. In this state, all inelastic  
2 two-body processes are endothermic and are thus fully  
3 suppressed at sufficiently low temperature. This state  
4 requires optical trapping since it cannot be captured  
5 in a magnetic trap. Optically trapped atoms can only  
6 be efficiently evaporated by lowering the total poten-  
7 tial depth. This process weakens the confinement of the  
8 trapped sample and thus makes it difficult to achieve  
9 sufficiently high elastic collision rates for effective evap-  
10 oration. Hence, adjustability of the collisional properties  
11 is very helpful for a fast evaporation strategy.

12 The success in condensing Cs [4] largely relies on the fact  
13 that the s-wave scattering length for the  $F = 3, m_F = 3$   
14 state can be tuned to moderate and positive values by  
15 the application of relatively low dc magnetic fields [13].  
16 As Fig. 1 shows, an external magnetic field allows for  
17 precise tuning of the atomic scattering length  $a$  from  
18 negative to positive values. Positive scattering lengths in  
19 the range between zero and one thousand  $a_0$  are attained  
20 for magnetic fields of a few ten Gauss;  $a_0$  denotes Bohr’s  
21 radius. In particular, there is a gentle zero-crossing of the  
22 scattering length near 17 G [25]. Here, the interaction  
23 of atoms in a BEC is effectively switched off. Several  
24 narrow higher-order Feshbach resonances [13], caused by  
25 coupling to d- and g-wave molecular states, enable very  
26 rapid control of the atomic scattering properties. With  
27 the magnetic field being a free parameter in our optical  
28 trapping approach, we can take full advantage of this  
29 tunability of the s-wave scattering length.

30 For Cs in the  $F = 3, m_F = 3$  ground state the process  
31 of three-body recombination is the dominant loss and  
32 heating mechanism [28]. In a recombination process,  
33 three atoms collide, two of them form a molecule, and  
34 the third atom takes away two thirds of the binding en-

ing off the reservoir trap excellent conditions for further  
forced evaporative cooling are obtained.

The different trap stages of optical trapping used in our  
experiments are illustrated in Fig. 2. An overview of the  
evolution of phase-space density and particle number for  
the various trapping stages is shown in Fig. 3.

The use of relatively weak optical trapping necessitates  
the implementation of magnetic “levitation” where a  
magnetic field gradient along the vertical direction com-  
pensates for the gravitational force. This levitation turns  
out to be very useful in two ways: First, in the limit of  
very weak optical trapping only one spin state is held  
in the trap. This assures perfect spin polarization of the  
sample<sup>1</sup>. Further, efficient evaporation can be performed  
without the effect of gravitational sag in the trap. The dc  
magnetic field offset remains a free parameter for flexible  
tuning of the scattering length.

### 3.2 Laser cooling

The initial collection and cooling of Cs atoms is achieved  
by conventional techniques. In a stainless steel vacuum  
chamber [32] atoms are loaded into a magneto-optical  
trap (MOT) from a Zeeman slowed atomic beam with  
up to  $3 \times 10^8$  atoms after about 6 s. The MOT is op-  
erated on the  $6^2S_{1/2}, F = 4$  to  $6^2P_{3/2}, F' = 5$  transi-  
tion. The ultra-high vacuum of less than  $1 \times 10^{-11}$  mbar  
gives 200 s for the  $1/e$ -lifetime of the MOT. The MOT  
light is derived from a high power laser diode<sup>2</sup> referenced  
via beat-lock to a grating-stabilized master diode laser.  
Standard absorption imaging is used to determine par-  
ticle numbers and temperatures.

We compress the atomic cloud by ramping up the mag-  
netic field gradient in the MOT by a factor of 5 to 33  
G/cm within 40 ms. Simultaneously we linearly change  
the detuning of the MOT laser from around 10 MHz  
to 30 MHz. At the end of the ramp, we switch off the  
MOT light and the magnetic field gradient. To cool the  
compressed cloud, we then apply degenerate Raman-  
sideband cooling [30] in an optical lattice to further cool  
and to polarize the atoms in the desired  $F = 3, m_F = 3$   
state. We have adapted the technique as described in [33]  
to our setup. This cooling scheme is particularly suited  
for polarizing atoms in the  $F = 3, m_F = 3$  state be-  
cause this is a dark state for which photon scattering is  
suppressed. Four laser beams derived from an injection  
locked slave laser resonant with the  $F = 4$  to  $F' = 4$   
transition produce a three-dimensional optical lattice,  
drive Raman-sideband transitions and repump out of  
the  $F = 4$  ground state manifold. The total power of  
all the four beams is 65 mW and their  $1/e^2$ -beam radii  
are about 1 mm. The oscillation frequency in the lat-  
tice is on the order of 100 kHz. A small magnetic field  
offset of several hundred mG is applied to induce the  
Raman-sideband cooling. We succeed in polarizing 90%  
of the atoms. The ensemble is then adiabatically released  
from the lattice after 6 ms of cooling time. If the atomic  
cloud is released into free space, the temperature of the

ensemble with up to  $4 \times 10^7$  atoms is about  $0.7 \mu\text{K}$ . For  
our typical atomic densities this corresponds to a phase  
space density of  $1 \times 10^{-3}$ .

### 3.3 Reservoir trap

We generate the large reservoir trap by horizontally cross-  
ing two CO<sub>2</sub>-laser beams A<sub>1</sub> and A<sub>2</sub> at right angles as  
shown in Fig. 2(a). At the same time we apply a mag-  
netic gradient field in the vertical direction to levitate  
the atoms against gravity. The delivered powers in laser  
beams A<sub>1</sub> and A<sub>2</sub> are 90 W and 65 W, respectively.  
The light comes from two separate, highly stable lin-  
early polarized single-frequency CO<sub>2</sub>-lasers<sup>3</sup>. Switching  
of the beams is done by external acousto-optical mod-  
ulators<sup>4</sup> (AOMs). A<sub>1</sub> is downshifted in frequency by 40  
MHz, whereas A<sub>2</sub> is upshifted by 40 MHz to prevent any  
interference. To avoid mode-hops the cooling water for  
the lasers needs to be stabilized to better than  $\pm 20$  mK.  
Still, a slow mode drift changes the power of the lasers  
by a few percent over the time scale of minutes. At the  
crossing point the  $1/e^2$ -beam radii of the two lasers are  
( $605 \pm 35$ )  $\mu\text{m}$  and ( $690 \pm 35$ )  $\mu\text{m}$ .

The magnetic fields for levitation and for Feshbach tun-  
ing are generated by two pairs of coils (aligned with their  
axes parallel to the vertical direction. One pair in anti-  
Helmholtz configuration produces the vertical magnetic  
field gradient near 31.3 G/cm to levitate the atoms in the  
 $F = 3, m_F = 3$  state. Another pair in Helmholtz config-  
uration provides a variable bias field  $B_0$  of up to 200 G.  
The combined field results in a weak outward directed  
force  $F(\rho) = m\alpha^2\rho$  depending on the horizontal distance  
 $\rho$  from the vertical symmetry axis. For perfect levitation  
of our atoms the constant  $\alpha = g\sqrt{m/(3\mu_B B_0)}$  describes  
the curvature of the parabolic anti-trapping potential.  
The levitation field thus slightly reduces the trap depth  
along the horizontal direction. Here,  $m$  is the mass of  
Cs,  $g$  is the gravitational acceleration, and  $\mu_B$  is Bohr’s  
magneton. At  $B_0 = 17$  G we have  $\alpha = 2\pi \times 3.4$  Hz. The  
horizontal trap frequencies  $\omega_{x,y}$  are reduced according  
to  $\omega'_{x,y} = \sqrt{\omega_{x,y}^2 - \alpha^2}$ . This is usually a very small effect  
for all but the lowest trap frequencies. Note that levi-  
tation also affects the horizontal motion of free atoms  
after the optical trap is shut off. The horizontal motion  
follows  $\rho(t) = \rho_0 \cosh(\alpha t) + \alpha^{-1}v_0 \sinh(\alpha t)$  for initial  
position  $\rho_0$  and initial velocity  $v_0$ . The vertical motion  
is not affected.

We excite vertical trap oscillations by briefly changing  
the vertical magnetic field gradient and hence tilting the  
trap. For exciting horizontal trap oscillations we shift the  
equilibrium position of the atoms by adding a horizon-  
tal magnetic field component. In both cases we monitor  
the center-of-mass oscillation of the atomic cloud after  
50 ms time-of-flight. The geometrically averaged trap  
frequency  $\bar{\nu}$  is calculated to be ( $12.6 \pm 1.5$ ) Hz which  
is in good agreement with the experimental value of  
( $13.2 \pm 0.2$ ) Hz. Together with the levitation and the  
magnetic bias field the lasers provide an effective trap

<sup>1</sup> This Stern-Gerlach separation technique also allows for  
radio-frequency evaporation along the vertical direction. Al-

<sup>3</sup> Coherent-DEOS GEM-100L

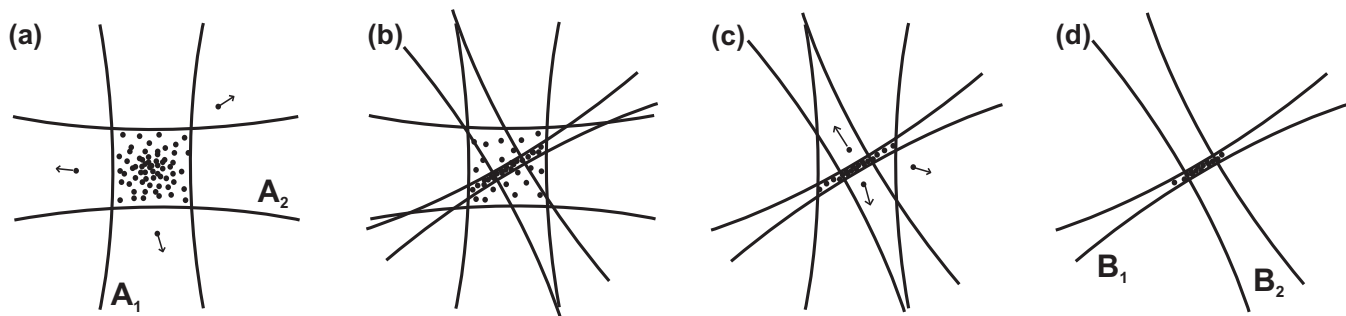


**Fig. 2** Illustration of the various stages of trap loading and evaporative cooling as seen from above. (a) Plain evaporation in a crossed CO<sub>2</sub>-laser trap generated by beams A<sub>1</sub> and A<sub>2</sub> at a scattering length of  $a = 1215 a_0$ . (b) 1.5 s of ramping and collisional loading into a crossed 1064-nm fibre laser trap generated by beams B<sub>1</sub> and B<sub>2</sub> with a final scattering length  $a = 210 a_0$ . (c) Forced evaporative cooling after switching off CO<sub>2</sub>-laser beam A<sub>2</sub>. The power of all remaining lasers is ramped down, and the power in CO<sub>2</sub>-laser beam A<sub>1</sub> is reduced to zero. (d) Final configuration of the crossed 1064-nm trap. Imaging is done in the horizontal plane at an angle of 30° with respect to the long axis of the cigar-shaped atomic cloud.

1 depth of about  $k_B \times 7 \mu\text{K}$ . This trap depth is given by 39  
 2 the weaker of the two CO<sub>2</sub>-lasers as the atoms can escape 40  
 3 along the direction of the stronger beam. 41

4 For transfer of the precooled atoms into the reservoir 42  
 5 trap, we leave the light of the two CO<sub>2</sub>-lasers on dur- 43  
 6 ing the entire pre-cooling phase. This is because the 44  
 7 CO<sub>2</sub>-lasers show strong variations in beam pointing and 45  
 8 beam shape as a function of radio-frequency power to 46  
 9 the AOMs. We have checked that the small light shift 47  
 10 introduced by the lasers does not affect the initial load- 48  
 11 ing and cooling efficiency. The reservoir trap is then acti- 49  
 12 vated by ramping up the magnetic field and its gradient. 50  
 13 The  $1/e$ -rise time of the magnetic fields is limited to 1.5 51  
 14 ms because of eddy currents in the stainless steel cham- 52  
 15 ber. We therefore do not expect the transfer to be fully 53  
 16 adiabatic. 54

17 We find that the atoms are heated to about  $2.2 \mu\text{K}$  by 55  
 18 the transfer into the reservoir trap. A clear measurement 56  
 19 on the trapped sample is only possible after about 50 ms 57  
 20 since the system initially is not in thermal equilibrium 58  
 21 and since the untrapped atoms need to disappear from 59  
 22 the field of view. We largely attribute the heating to im- 60  
 23 perfect phase space matching. In fact, the atomic cloud 61  
 24 after Raman-sideband cooling to  $0.7 \mu\text{K}$  has a  $1/e$ -radius 62  
 25 of  $\sim 350 \mu\text{m}$ . In comparison, an equilibrium distribution 63  
 26 in the reservoir trap at  $0.7 \mu\text{K}$  would have a  $1/e$ -radius 64  
 27 of  $\sim 100 \mu\text{m}$ . Potential energy is thus gained which is 65  
 28 then turned into kinetic energy, effectively heating the 66  
 29 cloud of atoms. Subsequently, the hot atoms evaporate 67  
 30 out of the trap. For this phase of plain evaporation we 68  
 31 set the magnetic bias field to 73.5 G. The scattering len- 69  
 32 gth is then  $1215 a_0$ . The temperature is reduced to less 70  
 33 than  $1 \mu\text{K}$  within 10 s. After this time, we measure more 71  
 34 than  $4 \times 10^6$  atoms, corresponding to a peak phase space 72  
 35 density of  $2 \times 10^{-3}$ . 73

### 3.4 Dimple trap 74

37 We proceed with loading of the dimple trap after 2 s of 75  
 38 plain evaporation in the reservoir trap. At this point the 76

atom number is  $7.8 \times 10^6$  and the phase space density is 89  
 $1.7 \times 10^{-3}$  (see Fig. 3). The dimple trap is generated by 90  
 horizontally intersecting one tightly focused laser beam 91  
 B<sub>1</sub> with  $34\text{-}\mu\text{m}$  waist and another less focused beam B<sub>2</sub> 92  
 with  $260\text{-}\mu\text{m}$  waist at right angles, rotated by 30° in the 93  
 horizontal plane with respect to the CO<sub>2</sub>-laser beams 94  
 as shown in Fig. 2(d). This is different from our ear- 95  
 100 lier work [4] where we have used CO<sub>2</sub>-laser beam A<sub>2</sub> for 96  
 axial confinement. We introduce the B<sub>2</sub> beam because 97  
 some weak back reflections of the CO<sub>2</sub>-laser beams led 98  
 to a slight undesirable corrugation of the optical poten- 99  
 100 tial. This complicated the quantitative analysis of the 101  
 BEC. Beams B<sub>1</sub> and B<sub>2</sub> are derived from a broadband 102  
 fiber laser<sup>5</sup> at 1064 nm. The powers in these beams are 103  
 ramped up within 1.5 s to a maximum power of 70 mW 104  
 for B<sub>1</sub> and 270 mW for B<sub>2</sub>. The trapping in the dimple 105  
 is now briefly done by all four laser beams with B<sub>1</sub> provid- 106  
 ing most of the radial and A<sub>1</sub> most of the axial confine- 107  
 ment. After switching off beam A<sub>2</sub> we measure the radial 108  
 and axial trap frequencies in the dimple to  $(221.2 \pm 1.6)$  109  
 Hz and  $(14.2 \pm 0.1)$  Hz, respectively. During the ramp- 110  
 ing up phase of B<sub>1</sub> and B<sub>2</sub> we reduce the magnetic field 111  
 offset to 23 G and thus the scattering length to  $300 a_0$  112  
 in order to reduce losses from three-body recombination 113  
 [28]. The trap now contains about  $1.7 \times 10^6$  atoms at a 114  
 peak phase space density of approximately 0.13. 115

### 3.5 Forced evaporation towards BEC 116

We start forced evaporative cooling by ramping down 117  
 the power in all three remaining beams. Simultaneously 118  
 we remove the reservoir by switching off the CO<sub>2</sub>-laser 119  
 A<sub>2</sub> that is not responsible for axial confinement. To as- 120  
 121 sure a well-defined ramp over a large intensity range we 122  
 control the light power of the near-infrared beam B<sub>1</sub> by 123  
 means of a logarithmic photodiode and a servo loop. The 124  
 power in CO<sub>2</sub>-laser beam A<sub>1</sub> is ramped to zero within 125  
 5.5 s so that B<sub>2</sub> at the end of evaporation exclusively as- 126  
 127 sures axial confinement. The change in beam pointing for 128  
 A<sub>2</sub> does not affect the evaporation. For B<sub>1</sub> we approxi- 129

<sup>5</sup> IPG Laser PYL-10

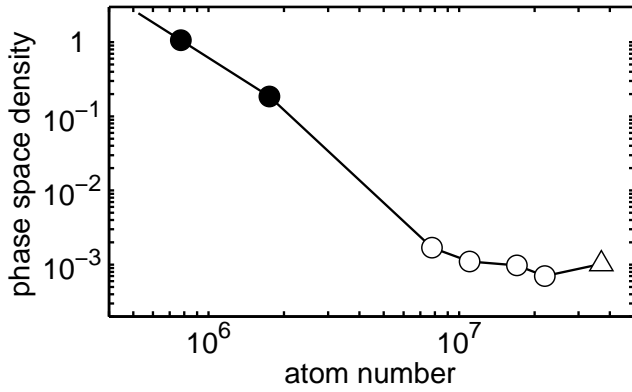


**Fig. 3** Peak phase space density as function of atom number. The path of evaporation proceeds from right to left. The *triangle* shows the atomic ensemble immediately after lattice cooling. The *open circles* show the ensemble in the reservoir trap after 0.08, 0.22, 0.64, and 2.0 s. The *filled circles* correspond to the sample in dimple trap right after loading and after 1.5 s of evaporation. The phase transition occurs after 2 s of forced evaporation with  $\sim 5 \times 10^5$  atoms left in the dimple trap.

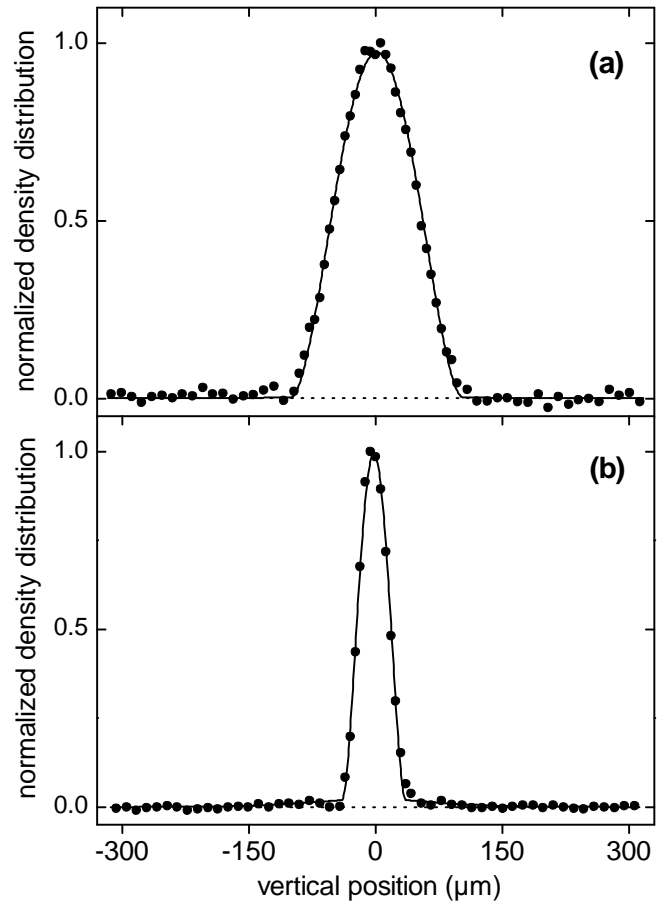


**Fig. 4** Vertical density profiles of Cs condensates after 100 ms of free expansion in the levitation field. The solid curves are fits to the data for the Thomas-Fermi profiles which include possible thermal components. For better distinction the baseline is dashed. (a) Expansion with no change in scattering length. The total number of atoms in the condensate is  $N = 1.1 \times 10^5$ . (b) Expansion near zero scattering length under the same conditions reveals a small thermal component with a temperature of about 10 nK.

1 mately follow an exponential ramp over 5.5 s. The power  
 2 in beam  $B_2$  is only slightly reduced. The final power in  
 3  $B_1$  and  $B_2$  is 0.5 mW and 220 mW. We find and optimize  
 4 this ramp by extending the ramp in discrete time steps  
 5 of a few hundred milliseconds at the beginning and up  
 6 to one second towards the end of the ramp.

7 At each step we search for a maximum in evaporation  
 8 efficiency  $\gamma = \log(D'/D)/\log(N/N')$  as a function of the  
 9 trap depth and scattering length [34]. Here,  $D$  and  $D'$   
 10 are the phase-space densities at the beginning and end  
 11 of each step,  $N$  and  $N'$  denote the respective particle  
 12 numbers. Maximizing  $\gamma$  at each step results in an overall  
 13 optimization of the evaporation path. We find that a  
 14 magnetic field value of 21 G with scattering length  $a =$   
 15  $210 a_0$  is optimal during the forced evaporation phase.  
 16 As can be seen from Fig. 3 the efficiency  $\gamma$  lies around  
 17 3 during the forced evaporation ramp. We attribute this  
 18 high efficiency to the fact that atoms can escape the trap  
 19 into almost all directions because of the levitation field.  
 20 We observe the phase transition after 2 s of forced evapo-  
 21 rative cooling with about  $5 \times 10^5$  atoms at a temperature  
 22 of  $(200 \pm 10)$  nK. At this point the power in beams  $B_1$   
 23 and  $B_2$  is 8.7 mW and 250 mW. The duration of the  
 24 ramp is relatively short. Our evaporation proceeds close  
 25 to the hydrodynamic regime. Thus, significant improve-  
 26 ment of the evaporation is not to be expected.

27 Further evaporation leaves a cigar-shaped condensate  
 28 with the long axis in the horizontal plane. In Fig. 4 we  
 29 show vertical density profiles of expanding condensates.  
 30 The tunability of the scattering length allows us to ex-  
 31 plore different regimes of expansion. For Fig. 4(a) we  
 32 expand the condensate at the creation scattering length  
 33 of  $210 a_0$ . This is the usual type of self-similar expansion  
 34 in which the condensate in the Thomas-Fermi regime re-

tains its parabolic shape [35]. For Fig. 4(b) we step the  
 scattering length to zero at the moment of release from  
 the trap. The mean-field interaction thus vanishes and  
 the rate of expansion is greatly reduced. This exposes a  
 small thermal component, for which a bimodal fit reveals  
 a temperature of around 10 nK. The critical tempera-  
 ture at these trapping conditions is 24 nK, therefore the  
 expected condensate fraction agrees well with the mea-  
 sured value of 91%. From the fit to the data in Fig. 4  
 we obtain that there are up to  $1.1 \times 10^5$  atoms in the  
 condensate with a 20% calibration error. The error does  
 not come from the fit but from the overall uncertainty in  
 determining the atom number. Usually, the error from  
 absorption imaging alone is around 50%, but we can cali-  
 brate the atom number from measurements on the chemi-  
 cal potential, see Sec. 4.1. For this particular experiment  
 we measure the final trap frequencies to  $(4.3 \pm 0.2)$  Hz

and  $(21.1 \pm 0.2)$  Hz along the axial and radial direction, respectively. We thus infer for the initial Thomas-Fermi sizes  $R_r^{TF} = (8.7 \pm 0.3) \mu\text{m}$  and  $R_a^{TF} = (42.5 \pm 1.2) \mu\text{m}$  along the radial and axial directions at a scattering length of  $a = 210 a_0$ . The peak density of the condensate is  $n_0 = (2.1 \pm 0.1) \times 10^{13} \text{ cm}^{-3}$ .

#### 4 Tunable quantum gas

We now test the tunability of the condensate interaction. We first study the condensate expansion as a function of scattering length [36] in two different ways. We then specialize to the case when the interaction energy is switched off and present improved results on the ultra-slow expansion of the condensate in comparison with earlier measurements in [4]. Finally, we excite compression oscillations of the trapped condensate by suddenly stepping the scattering length to a lower value.

##### 4.1 Expansion energy as a function of scattering length

We measure the release energy of the condensate for slow and fast changes of the scattering length. When we slowly vary the scattering length the wave function of the trapped condensate can follow adiabatically and the condensate remains in equilibrium. The release energy is proportional to the chemical potential of the condensate at the given value of the scattering length. The situation is different when we rapidly switch the scattering length at the moment of condensate release. The condensate then expands from a non-equilibrium state because the wave function has not had time to adjust to the change in interaction energy. This leads to strong changes for the rate of condensate expansion in comparison to the expansion from equilibrium.

We first consider a condensate in the Thomas-Fermi regime for which we adiabatically ramp the scattering length to a new value. For such a condensate, the release energy  $E_{rel}$  directly corresponds to the chemical potential  $\mu_{TF}$  through  $\frac{7}{2}E_{rel} = \mu_{TF}$  [35], which is given by

$$\mu_{TF} = \frac{\hbar \bar{\nu}}{2} \left( \frac{15 N}{a_{ho}} \right)^{2/5} a^{2/5}. \quad (1)$$

Here,  $\bar{\nu}$  is the geometric average of the trap frequencies,  $N$  is the particle number in the condensate, and  $a_{ho} = \sqrt{\hbar/(m 2\pi \bar{\nu})}$  is the oscillator length. For the experiment we produce a condensate with  $N = 8.5 \times 10^4$  atoms at a creation scattering length of  $a_c = 210 a_0$ . We then slowly ramp the magnetic field to values between 20 and 35 G, setting the scattering length to a value between about 200 and 700  $a_0$ . The slow ramping excludes values below the Feshbach resonance at 19.9 and above the one at 48.0 G because of strong loss<sup>6</sup>. The condensate is then released from the trap and we measure the release energy. The results are shown in Fig. 5. Here we assume that the magnetic field strength translates into scattering length according to Fig. 1. The data is well fit by a function of the form  $C a^{2/5}$  according to Eq. (1). From the fit parameter  $C$  we can deduce an independent

<sup>6</sup> A combination of slow ramping and quick jumping at the Feshbach resonances would allow access to the full range of

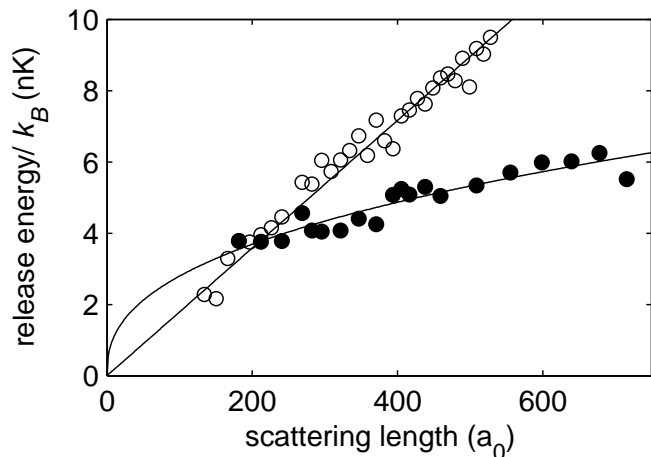


**Fig. 5** Release energy of the condensate as a function of scattering length  $a$ . The *filled circles* represent experimental data for the case of adiabatic ramping of a trapped condensate. The data, corresponding to  $2/7$  of the chemical potential at a given value of the scattering length, is fit by  $C a^{2/5}$ . The *open circles* represent data for rapid switching at the moment of condensate release. As discussed in the text, the straight line is not a fit. It connects the origin with the fitted value of the release energy at the creation scattering length.

estimate of the particle number  $N = (8.2 \pm 1.3) \times 10^4$ . The error is dominated by the error in determining the trap frequencies.

For a sudden change of the scattering length the condensate wave function has no time to react. For example, for an increase of the scattering length the density distribution is too narrow in comparison to the equilibrium density distribution at the new value of the scattering length. The condensate thus expands more rapidly than a condensate in equilibrium at this new value. Since the mean-field interaction energy of the condensate scales linearly with the scattering length for a given density profile [35], we expect a linear behavior of the release energy as a function of the final scattering length  $a$ . In Fig. 5 we thus compare the data for the measured release energy to a straight line  $C a_c^{2/5} a/a_c$  given by the origin and the fitted value of the release energy at the creation scattering length  $a_c = 210 a_0$ . We find good agreement with the linear dependence.

##### 4.2 Ultra-slow condensate expansion

We now study the expansion of the condensate near the zero-crossing of the scattering length. At the moment of condensate release, we rapidly switch the magnetic field from the creation field near 20 G to  $(17.17 \pm 0.05)$  G, corresponding to  $a = (3.4 \pm 3.0) a_0$ . The error in determining the precise magnetic field at the position of condensate requires that we choose a slightly positive value of the scattering length to assure that no weakly attractive interactions modify the condensate expansion. The levitation field remains on, allowing for an extended observation period because the atoms then do not fall under

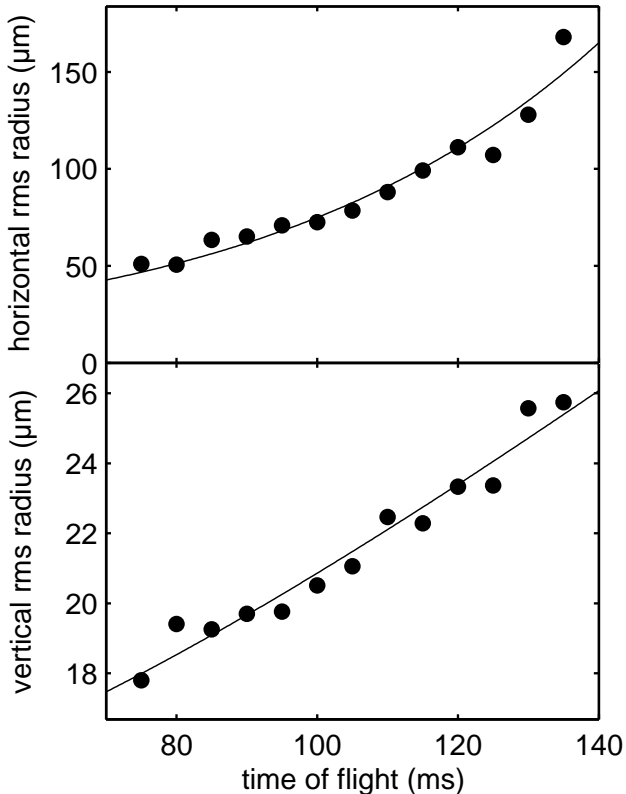


**Fig. 6** Expansion of the non-interacting condensate. The data points show the horizontal (above) and vertical (below) rms radius of the BEC as a function of expansion time near the zero crossing of scattering length. Note the different scales. The fit to the residual vertical expansion reveals a release energy of  $k_B \times (51 \pm 3)$  pK. For the horizontal expansion the data is fit by  $A \cosh(\alpha t)$  with  $\alpha = 2\pi \times (3.20 \pm 0.23)$  Hz.

gravity. Fig. 6 shows the vertical and horizontal extent of a BEC with  $1.2 \times 10^5$  atoms as a function of time after release from the trap. We only show the data after 75 ms of expansion when the optical density of the atomic cloud is sufficiently reduced to allow for reliable absorption imaging. The horizontal expansion is dominated by the magnetic anti-trapping potential which derives from the presence of the levitation field and which magnifies the atomic cloud according to the cosine hyperbolicus function, see Sec. 3.3. The measured rate of expansion  $2\pi \times (3.20 \pm 0.23)$  Hz agrees reasonably well with the expected rate constant  $\alpha = 2\pi \times 3.4$  Hz. The vertical expansion corresponds to a release energy of  $k_B \times (51 \pm 3)$  pK. Note that this is much lower than the kinetic energy of the ground state  $\hbar\omega_r/4 = k_B \times 253$  pK given by a radial trap frequency of  $\omega_r = 2\pi \times 21.1$  Hz. It is remarkable that the release energy is less than the zero-point energy of the ground state. Since the spatial extent of the condensate is much larger than the size of the ground state wave function of the harmonic oscillator, the momentum spread, limited by the uncertainty of the wave function

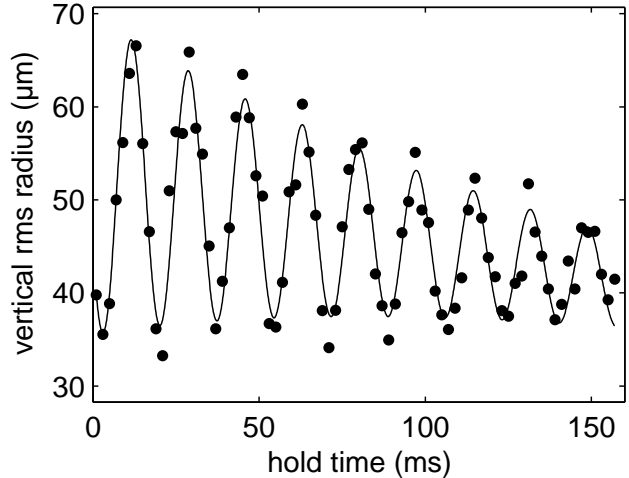


**Fig. 7** Condensate oscillations after rapid switching of the scattering length. The filled circles show the vertical rms radius of an expanding BEC with  $7 \times 10^4$  atoms after 80 ms of free expansion as a function of hold time in the trap. The scattering length has been switched rapidly from  $363 a_0$  to  $25 a_0$ . The solid curve is a fit to the data giving an oscillation frequency of  $(58.3 \pm 0.2)$  Hz. We independently measure the radial trap frequency to  $(28 \pm 1)$  Hz.

of the initial condensate, is lower than that of the ground state.

#### 4.3 Condensate oscillations

By rapidly ramping the scattering length it is possible to excite oscillations of the condensate in the trap [37]. In fact, in the limit of a cigar shaped condensate one expects radial “compression” or “expansion oscillations” at twice the trap frequency. Compression oscillations can be seen in Fig. 7 where we plot the vertical radius of the released condensate as a function of hold time  $t_h$  in the trap. To excite the oscillation we step the scattering length from a value of  $a = 363 a_0$  ( $B = 24.4$  G) to  $a = 25 a_0$  ( $B = 17.6$  G) at time  $t_0$ . The condensate is then allowed to oscillate in the trap for a variable hold time  $t_h$  at the final value of the scattering length. We release the condensate at time  $t_0 + t_h$  and take an image after 80 ms of free expansion. We fit the data by a sinusoidal function. The measured compression oscillation frequency of  $(58.3 \pm 0.2)$  Hz agrees well with twice the radial trap frequency of  $2 \times (28 \pm 1)$  Hz at the given trapping power. To account for the damping we have to introduce an exponential decay of the amplitude and of the offset value. The damping of the amplitude has a time constant of 126 ms. We have not yet identified the origin of this damping. Possibly the BEC samples different trapping frequencies due to the large amplitude of the oscillation, which would lead to an apparent damping. Also, damping might be caused by the interaction



with a residual thermal cloud or by parametric processes [38].

## 5 Conclusion

We have shown that essentially pure Cs condensates can be produced with more than  $10^5$  atoms. In our optical trap it is possible to flexibly change the atomic scattering properties. The atomic condensate can now be used as the starting point for experiments where a tuning and ramping of the scattering properties can be exploited. It will be interesting to study the case of a non-interacting condensate at the zero-crossing of the scattering length. Such a condensate might be used in atom interferometers where one wishes to suppress any mean-field effects [39]. On the other hand, tuning to large values of the scattering length might allow the investigation of effects beyond the mean-field approximation [35]. Also, modulation of the scattering length could be used as an alternative tool to probe the excitation spectrum of the condensate. Finally, ultracold Cs<sub>2</sub> molecules can be created by ramping across one of the Feshbach resonances [8] and the transition from an atomic to a molecular condensate could then be studied.

**Acknowledgements** This work is supported by the Austrian “Fonds zur Förderung der wissenschaftlichen Forschung” (FWF) within SFB 15 (project part 16) and by the European Union in the frame of the Cold Molecules TMR Network under Contract No. HPRN-CT-2002-00290. M.M. is supported by DOC [Doktorandenprogramm der Österreichischen Akademie der Wissenschaften]. C.C. is supported by a Lise-Meitner-Fellowship from the FWF.

## References

1. M. Barrett, J. Sauer, M. Chapman: Phys. Rev. Lett. **87**, 010404 (2001)
2. Y. Takasu, K. Maki, K. Komori, T. Takano, K. Honda, M. Kumakura, T. Yabuzaki, Y. Takahashi: Phys. Rev. Lett. **91**, 040404 (2003)
3. G. Cennini, G. Ritt, C. Geckeler, M. Weitz: Phys. Rev. Lett. **91**, 240408 (2003)
4. T. Weber, J. Herbig, M. Mark, H.-C. Nägerl, R. Grimm: Science **299**, 232 (2003)
5. D. Rychtarik, B. Engeser, H.-C. Nägerl, R. Grimm: Phys. Rev. Lett. **92**, 173003 (2004)
6. C. Chin, A. J. Kerman, V. Vuletic, S. Chu: Phys. Rev. Lett. **90**, 033201 (2003)
7. C. A. Regal, C. Ticknor, J. L. Bohn, D. S. Jin: Nature **424**, 47 (2003)
8. J. Herbig, T. Kraemer, M. Mark, T. Weber, C. Chin, H.-C. Nägerl, R. Grimm: Science **301**, 1510 (2003)
9. S. Dürr, T. Volz, A. Marte, G. Rempe: Phys. Rev. Lett. **92**, 020406 (2004)
10. K. Xu, T. Mukaiyama, J. R. Abo-Shaeer, J. K. Chin, D. E. Miller, W. Ketterle: Phys. Rev. Lett. **91**, 210402 (2003)
11. S. Jochim, M. Bartenstein, A. Altmeyer, G. Hendl, S. Riedl, C. Chin, J. Hecker Denschlag, R. Grimm: Science **302**, 2101 (2003)
12. M. Greiner, C. A. Regal, D. S. Jin: Nature **426**, 537 (2003)
13. C. Chin, V. Vuletic, A. J. Kerman, S. Chu, E. Tiesinga, P. J. Leo, C. J. Williams: Phys. Rev. A to appear
14. E. A. Donley, N. R. Claussen, S. T. Thomson, C. E. Wieman: Nature **417**, 529 (2002)
15. L. Radzihovsky, J. Park, P. B. Weichman: Phys. Rev. Lett. **92**, 160402 (2004)
16. M. W. J. Romans, R. A. Duine, S. Sachdev, H. T. C. Stoof: Phys. Rev. Lett. **93**, 020405 (2004)
17. J. Söding, D. Guéry-Odelin, P. Desbiolles, G. Ferrari, J. Dalibard: Phys. Rev. Lett. **80**, 1869 (1998)
18. J. Arlt, P. Bance, S. Hopkins, J. Martin, S. Webster, A. Wilson, K. Zetie, C. J. Foot: J. Phys. B **31**, L321 (1998)
19. D. Guéry-Odelin, J. Söding, P. Desbiolles, J. Dalibard: Europhys. Lett. **44**, 26 (1998)
20. D. Guéry-Odelin, J. Söding, P. Desbiolles, J. Dalibard: Optics Express **2**, 323 (1998)
21. S. A. Hopkins, S. Webster, J. Arlt, P. Bance, S. Cornish, O. Maragò, C. J. Foot: Phys. Rev. A. **61**, 032707 (2000)
22. P. J. Leo, E. Tiesinga, P. S. Julienne, D. K. Walter, S. Kadlecek, T. G. Walker: Phys. Rev. Lett. **81**, 1389 (1998)
23. A. M. Thomas, S. Hopkins, S. L. Cornish, C. J. Foot: J. Opt. B **5**, S107 (2003)
24. H. Perrin, A. Kuhn, I. Bouchoule, C. Salomon: Europhys. Lett. **42**, 395 (1998)
25. V. Vuletić, A. J. Kerman, C. Chin, S. Chu: Phys. Rev. Lett. **82**, 1406 (1999)
26. M. Hammes, D. Rychtarik, V. Druzhinina, U. Moslener, I. Manek-Hönninger, R. Grimm: J. Mod. Opt. **47**, 2755 (2000)
27. D.-J. Han, M. T. DePue, D. S. Weiss: Phys. Rev. A **63**, 023405 (2001)
28. T. Weber, J. Herbig, M. Mark, H.-C. Nägerl, R. Grimm: Phys. Rev. Lett. **91**, 123201 (2003)
29. D. J. Han, Marshall T. DePue, David S. Weiss: Phys. Rev. A **63**, 023405 (2001)
30. A. J. Kerman, V. Vuletić, C. Chin, S. Chu: Phys. Rev. Lett. **84**, 439 (2000)
31. D. M. Stamper-Kurn, H.-J. Miesner, A. P. Chikkatur, S. Inouye, J. Stenger, W. Ketterle: Phys. Rev. Lett. **81**, 2194 (1998)
32. T. Weber: PhD thesis, Univ. Innsbruck 2003
33. P. Treutlein, K. Y. Chung, S. Chu: Phys. Rev. A **63**, 051401 (2001)
34. W. Ketterle, N. J. Van Druten: Adv. At. Mol. Opt. Phys. **37**, 181 (1996)
35. L. Pitaevskii, S. Stringari: *Bose-Einstein Condensation* (Clarendon Press, Oxford 2003)
36. S. L. Cornish, N. R. Claussen, J. L. Roberts, E. A. Cornell, C. E. Wieman: Phys. Rev. Lett. **85**, 1795 (2000)
37. Y. Kagan, E. L. Surkov, G. V. Shlyapnikov: Phys. Rev. Lett. **79**, 2604 (2001)
38. F. Chevy, V. Bretin, P. Rosenbusch, K. W. Madison, J. Dalibard: Phys. Rev. Lett. **88**, 250402 (2002)
39. S. Gupta, K. Dieckmann, Z. Hadzibabic, D. E. Pritchard: Phys. Rev. Lett. **89**, 140401 (2002)